# Real Space Demonstration of Induced Crystalline 3D Nanostructuration of Organic Layers

*Markos Paradinas,*[a,‡] *Ana Pérez-Rodríguez,*[a] *Esther Barrena*[a*] *and Carmen Ocal*[a]

[a]Institut de Ciència de Materials de Barcelona (ICMAB-CSIC), Campus UAB, Bellaterra 08193-Barcelona, Spain

ABSTRACT: The controlled 3D nanostructuration of molecular layers of the semiconducting molecules $C_{22}H_{14}$ (pentacene) and N, N'-dioctyl-3, 4, 9, 10-perylene tetracarboxylic diimide (PTCDI-C8) is addressed. A tip-assisted method using atomic force microscopy (AFM) is developed for removing part of the organic material and relocating it in up to six layers thick nanostructures. Moreover, unconventional molecular scale imaging combining diverse friction force microscopy modes reveals the stacking sequence of the piled layers. In particular, we unambiguously achieve epitaxial growth, an issue of fundamental importance in thin film strategies for the nanostructuration of more efficient organic nanodevices.

## Introduction

Soft materials comprised of low molecular weight organic molecules are attracting increasing interest because of their importance in the development of a number of emerging areas in nanoscience and technology, including molecular electronics, nanosystems for energy conversion and devices in the widest sense. Although nanodevices are still in an early stage of development, future research in the field will have to face the requirement of devices integration and miniaturization as already occurred in silicon based technologies. For this realization, it is essential the development of tools that enable nanofabrication and material manipulation with nanometer precision.

Among the variety of applications of scanning probe microscopy (SPM), the scanning probe lithography (SPL) techniques constitute a powerful approach for structuring surfaces at the nanometer scale.[1–3] SPL possess the versatility of locally modifying a wide range of different materials such as metals, organic molecules, polymers and biological molecules. Moreover, despite its known manufacturing speed limits, SPM combines the capability of both, fabrication and characterization. Many SPL methods have been developed in the last decades including either mechanical or electrical assisted processes, nanomanipulation,[4] dip-pen nanolithography (DPN),[5] scratching,[6,7] nanografting,[8] pressure induced restructuring,[9,10] electropeeling[11] or bias assisted electrostatic lithography,[12] local oxidation[13] and local resistive state manipulation[14] among others.

In this work, we present a different utility of SPM to locally induce the crystalline growth of diverse organic thin films. For its demonstration we have selected here two archetypal

semiconducting molecules considered as benchmarks in organic thin film transistors (OFETs): i) Pentacene ($C_{22}H_{14}$), a polycyclic aromatic hydrocarbon consisting of five linearly-fused benzene rings, which shows a preferential p-type behavior and a relative high field effect mobility[15] and ii) N'-dioctyl-3,4,9,10-perylene tetracarboxylic diimide (PTCDI-C8), which has an intrinsic interest as material for n-channel OFETs[16–20] and provides a largely anisotropic surface structure that enables accurately investigating the crystallinity of the organic layers by means of friction force microscopy (FFM) and transverse shear microscopy (TSM).[21]

The procedure presented here is proposed as a nanolithography approach for nanostructuration while ensuring the crystallographic quality of thin films for future organic nanodevices.

**Experimental methods**

Thin films of nominal thickness of few monolayers (ML) consisting of pentacene or PTCDI-C8 layers were deposited on top of Si substrates covered by a thin native $SiO_2$ layer. The substrates were cleaned by successive sonication cycles in acetone and ethanol ( ~ 5 minutes each) before being transferred to a devoted ultra-high vacuum (UHV) chamber where they were annealed at a temperature of ~300°C for 1h. The molecules were deposited by the organic molecular beam deposition (OMBD) in the same UHV chamber, typically at pressures in the range of $10^{-8}$ mbar. Prior to sample preparation, the growth parameters were optimized by a previous calibration to determine exposure time, rate deposition and substrate temperature. The pentacene thin films were grown at a substrate temperature of ~ 25°C and a deposition rate of ~0.2 ML per minute. The PTCDI-C8 thin films were grown at a substrate temperature of ~100°C at a rate of ~1.4 ML per minute.

The measurements presented here were performed in the load controlled contact mode atomic force microscopy (cm-AFM) mode at room temperature and for two relative humidity (RH) ranges: ambient conditions (typically RH ≈60-80%) and under $N_2$ environment reaching RH< 5%. Tips mounted in nominal low force constant (k=0.1-0.5 $Nm^{-1}$) V-shaped cantilevers were employed. AFM data were obtained with a commercial instrument from Nanotec Electrónica and analyzed with the WSxM freeware.[22] Lateral force imaging was performed in the friction force (FFM) and torsional shear (TSM) modes, where the tip scans perpendicular and parallel to the cantilever axis, respectively.[23–25]

**Results and discussion**

Pentacene films on $SiO_2$ exhibit the so-called thin film structure, with a layer spacing of ≈ 1.55 nm and molecules tilted ≈ 21° respect to the vertical. The molecules adopt a herringbone packing motif within the plane.[26] The pentacene monolayer (ML) on $SiO_2$ forms a slightly different crystalline structure with a nearly upright-standing orientation of the molecules[26–28] and a reported height of ≈ 1.60 ± 0.06 nm. Figure 1a shows the characteristic surface of pentacene deposits at coverages of ≈ 0.8 ML. Note that three surface levels exist due to the formation of second layer regions (light color) on top of large areas of the first molecular layer (intermediate color) leaving uncovered bare substrate regions (dark color). The second layer growth before the monolayer completion, i.e., growth of pentacene on pentacene already indicates that during OMBD the initial layer by layer growth converts to a much faster, ascribed to a defect assisted growth.[24] Intra-layer grain boundaries and new nucleation sites may lead to the formation of intra-layer domains and stacking faults (or even dislocations) influencing the thin film crystallinity.[24,29,30] The investigation of the local frictional properties by means of FFM has

shown to be a valuable tool for revealing structural details of molecular films,[21,31–33] which are difficult to visualize with other techniques and ultimately due to the stick-slip mechanism at atomic scale.[34] This technique has been exploited during the controlled manipulation described here to evidence structural domains and layer stacking; therefore, surface morphology and frictional response were verified at every stage of the process. Moreover, to avoid undesired film perturbation during monitoring (prior to and at the end of nanostructuration), the applied normal force ($F_n$) was maintained in the attractive regime (net negative load). Along the experiments, the tip-sample conditions were periodically checked by means of force-displacement curves, $F_n(z)$, in order to ensure adequate measuring conditions.

The protocol to transfer molecules from one surface location to another one without modifying the molecular film pre-existing in the new place is illustrated in Figure 1.

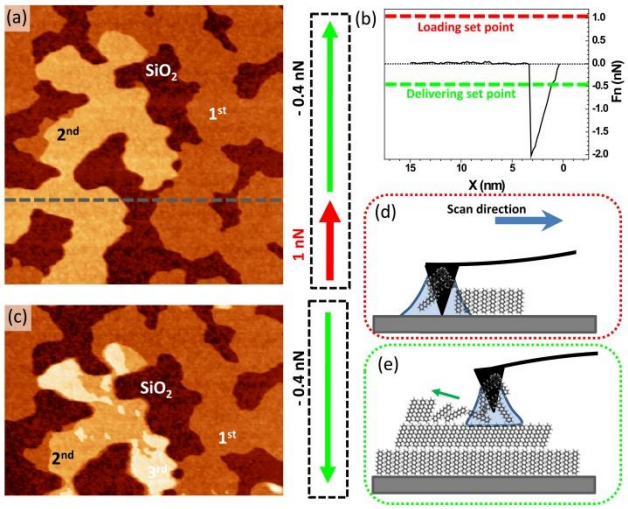


**Figure 1**.(a) cm-AFM topographic image prior to nanostructuration obtained at the pull off force. Red and green arrows along the slow scan direction refer to applied forces during slow scan travel. Image size: 1.3µm × 1.3µm. Total z scale: 5 nm. (b) Loading (red dashed line) and releasing (green dashed line) regimes are indicated in the $F_n(z)$ curve. (c) cm-AFM topographic image of the delivering region after 44 cycles of nanostructuration. (The image covering the

same lateral dimensions that in (a) is given in the Figure S1 of the Supporting Information). Total z scale of (a) and (c): 7 nm. (d) and (e) Sketch proposing the role of the water meniscus in the mechanism of loading and delivering plus spontaneous assembling of molecules (see text).

The selected surface region (Figure 1a) is imaged at the lowest practical load (pull off). Then, the area is scanned in a two-step sequence, from bottom to top and viceversa. During the scan travel (upwards in Figure 1b) the applied load is first set at a given value $F_n \approx 1$ nN, indicated in red, and then released to $F_n \approx -0.5$ nN (green) from the gray dashed line until the top. It is important to note that, in this particular experiment, these loads correspond to repulsive and attractive regimes, respectively (Figure 1b). As it will be demonstrated next, each regime corresponds to: i) Loading (red dashed), the pentacene molecules are collected from the surface by scanning in the repulsive regime and ii) delivering (green dashed), the molecules are transferred back to the surface by scanning in attractive conditions. A plausible mechanism is suggested in the figure sketch: Material removed from the lower region (Figure 1d) would be transferred to the upper part (above the gray dashed line) where the delivered molecules spontaneously re-assemble (Figure 1e). The practice can be repeated as many times as desired. Figure 1c shows the described procedure after 44 load-delivering cycles, where the growth of a third level of molecules can be clearly seen. Description of the induced process and the subsequent film characteristics are given in detail below.

Provided the properties of the growth material would depend on the crystallinity of the new nanostructured film, this issue is addressed here by jointly analyzing structural and frictional particularities in the delivering region. In order to that, the result of the described protocol before and after 23 load-delivering cycles is presented in Figure 2.

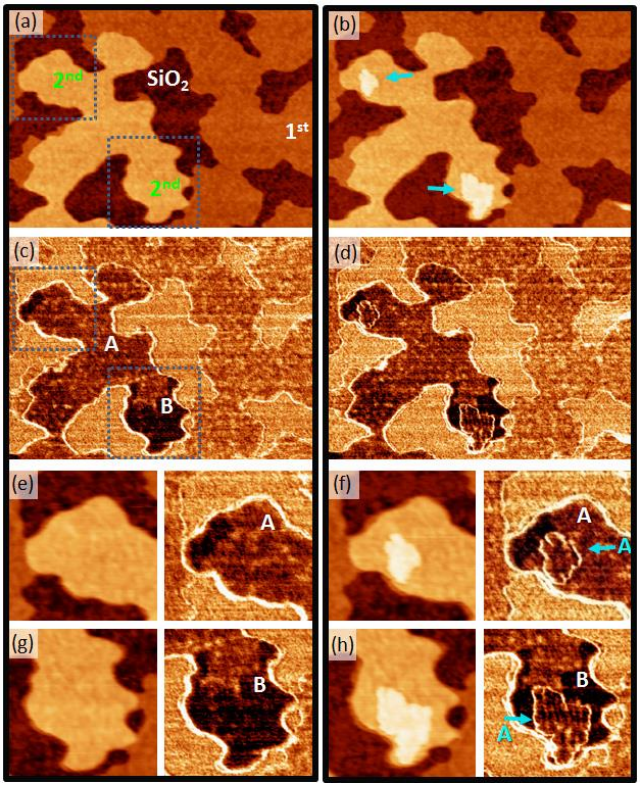


**Figure 2**. cm-AFM topography and simultaneous friction images determined from back and forth lateral force images (see Supporting Information Figure S2) of the delivering region at two stages of the induced pentacene growth. Initial (a,c) and after 23 load-delivering cycles (b, d). Dimensions: 1.3 μm × 0.87 μm. Elapsed time: ~14 minutes. Details of the film evolution (see text) are illustrated by the magnified images (e-h) corresponding to the areas marked in (a) and (c). Total z scale: 7 nm for (a, b, e, f, g, h).

The initial surface (Figure 2a) coincides with the corresponding upper region of Figure 1a. The first indication of a 3$^{rd}$-layer formation after manipulation is revealed by the detection of small islands in topography, indicated by cyan arrows in Figure 2b. It is noteworthy that the delivered molecules do not nucleate on the bare $SiO_2$, which remain as uncovered as in the as-prepared

OMBD film. Moreover, the formation of the 3rd level is absolutely favored with complete absence of enlargement of the 2nd layer pre-existing islands by any nucleation and assembling at their perimeters. However, comparison between Figure 2b and Figure 1c evidences that subsequent load-delivering cycles lead to a lateral growth of the newly nucleated islands and eventually to multilayer growth (see below).

Valuable crystallographic information can be obtained from the friction data. In the as-prepared sample (Figure 2c) the light regions correspond to the uncovered $SiO_2$ and the pentacene layers are distinguished by the lower friction sensed by the tip on them. Actually, the friction contrast between monolayer and bilayer can be related to the different tilt angle of the pentacene molecules in the first and second layers, in analogy with observations for other self-assembled organic systems.[35] It is outstanding that while the first molecular level of pentacene exhibits a quite homogeneous friction, the 2nd layer of the as-deposited pentacene presents intra-layer frictional contrast (see also Figure S2 in the Supporting Information). This fact is typical of the existence of structural domains, labeled as A and B in Figure 2c, and can be attributed to friction anisotropy (AN), i.e., to a different resistance to tip sliding for different azimuthal orientations of the pentacene domains.[35] Even though the monolayer may also consists of domains with diverse azimuthal orientation,[23] any variation in the frictional signal seems to be below our detection threshold. These different observations seem to be related with the nearly-vertical orientation of pentacene molecules in the first layer, leading to small AN, in contrast to the tilted configuration they adopt in the second layer, where an enhanced azimuthal contribution to the AN response of the sliding tip is expected.[32,36]

Inspection of the magnified friction images in Figures 2e-2h procures a deeper understanding of the particularities of the pentacene film during the induced growth. The friction observed for the new assemblies forming the 3rd layer is similar to that as-grown pentacene in the 2nd layer, giving evidence of the crystalline nature. As before mentioned, specific differences in friction can be ascribed to differences in the azimuth orientation of the domains or tilt variations for subsequent layers (more pronounced between the first and second pentacene layer). By the direct comparison between topography and friction before and after the nucleation of 3rd layer islands, one observes that the island on top of the region labeled as A presents the same friction than the underlying domain (A/A). This suggests registry between the 3rd and 2nd layers. However, the island nucleated on top of the domain labeled as B, is distinguished from the underlying layer by a different friction signal (A/B). This fact points to a different azimuthal orientation of the 3rd layer island in relation with the underlying pentacene in this particular region. Importantly, under our detection limit, the friction contrast in the 3rd layer is maintained during further tip-induced growth of the islands (see Figure S3 in the Supporting Information) indicating good thin film crystallinity.

The particular experiment of tip-induced growth presented here (215 load-delivering cycles) resulted in a multilayer formation of pentacene. The whole sequence of the process was monitored at each step and is summarized in Figure 3 by selected images corresponding to the first (a), intermediate (b) and final (c) stages of the experiment. A multi-color scale has been chosen to highlight the different layers. The amount of growing material (coverage) at each molecular layer has been quantified from the images height histograms and represented in the bars plot of Figure 3d. Note that up to six molecular levels are seen. An extended version of

Figure 3 is presented in Figure S4 where more steps of the tip-induced growth experiments are presented.

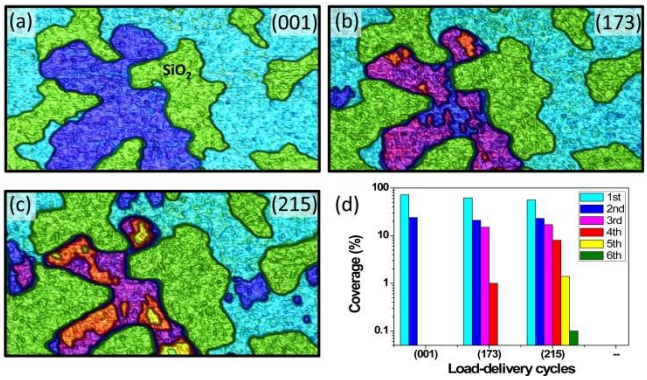


**Figure 3**. Topographic images of the initial (a), intermediate (b) and final (c) stages of the tip-induced growth of pentacene on $SiO_2$. The images correspond to frames number 1, 173 and 215 from a total of 215. Total elapsed time: ~ 2 h. The coverage for each molecular level is given by the bar plot in (d). The color code is the same as in the images.

We propose that the water meniscus has a role in the mechanism by which the pentacene molecules are transferred from one location to the other. The process is somehow similar to that at the basis of thee dip-pen nanolitograhy[5,37] and is schematically shown in Figures 1d and 1e. When the surface is scanned in a repulsive regime condition (positive loads), the molecular packing is destroyed (Supporting Information), the pentacene molecules are collected in the water meniscus formed in the tip-sample contact and dragged as an ink with a brush (situation a in figure 1d). In this sense, the important role of the lateral force is confirmed by the fact that the transport and growth of the organic layer does not occur when measuring in dynamic mode.

We tested the influence of water by changing the relative humidity from low humidity (RH < 5% maintained overnight) to ambient conditions (RH ≈ 60-80%). Even if a difference in the

water meniscus size is expected, no evidence of a different amount of transferred material was detected in the analyzed regime. Given that a water layer is not completely eliminated by lowering the humidity at room temperature, a conclusive test would only be obtained by in-situ measuring the grown films under UHV conditions or, conversely, by complete removal of capillary forces by measuring in liquid water.[38]

In order to further explore the viability of the tip-induced mechanism for general organic controlled growth and further aspects of the molecular crystallinity of the formed thin films, we performed similar experiments with PTCDI-C8, a molecule with a completely different chemical nature than pentacene. PTCDI-C8 is a liquid crystalline perylene derivative that organizes with highly crystalline packing.[19,20] We selected this system because of the large frictional anisotropy observed in PTCDI-C8 films allows identifying the azimuthal orientation of the molecular domains.[21] When sublimated onto $SiO_2$ substrates, PTCDI-C8 molecules self-assemble in a nearly perfect layer-by-layer fashion forming a smooth layered film.[39,40] Here, the initial surface consisted in a three monolayers thick thin film deposited by OMBD with no bare substrate exposed at the surface. The characteristic layered morphology of PTCDI-C8 films can be observed in Figure 4a, where the 3$^{rd}$-layer appears partially covered by 4$^{th}$-layer islands. The height of the PTCDI-C8 layer, as seen in the profile in Figure 4b, is consistent with previous reports.[6,41] Within each layer, PTCDI-C8 forms a slipped co-facial packing driven by the $\pi$- $\pi$ stacking between molecules.

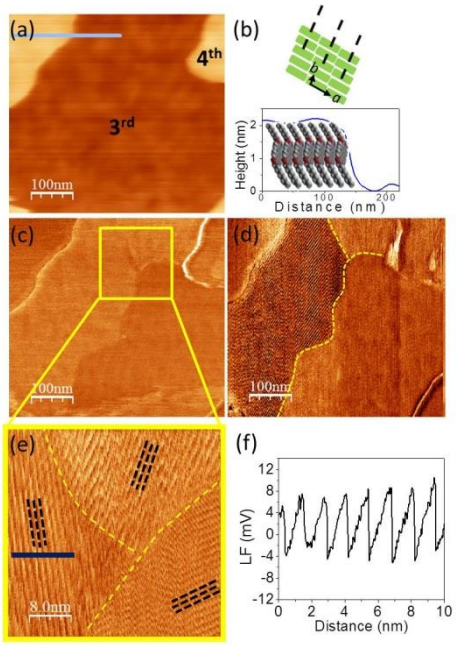


**Figure 4**: (a)Topographic image of the PTCDI-C8 film on $SiO_2$. (b) In-plane top view scheme (up) and height profile along the marked line in (a). Lateral force obtained in FFM (c) and in TSM (d). (e) High magnification image of the marked area. The molecular orientation for each domain is indicated by dashed black lines. (f) Profile of the lateral force (LF) along the blue line in (e).

A top-view representation of the in-plane lattice is shown in the scheme in Figure 4b. Images of the same area scanned in the conventional (FFM) and in the transverse (TSM) frictional modes, are shown in Figures 4c and 4d, respectively. The identification of rotational domains in these large-scale images is clearer when TSM is employed, a mode in which the sliding direction is parallel to the cantilever axis.[21] In fact, whereas the FFM image only reveals slight contrast between some of the crystalline domains, note that TSM provides high-contrast making visible domain boundaries not observed in FFM. The large variety of contrasts in TSM is correlated with the different azimuthal orientation of the domains with respect to the scanning direction. The structure in each domain has been deciphered by obtaining molecular resolution images in

both modes, as in detail reported in a previous work.[21] This is illustrated in Figure 4e showing three adjacent domains, in which the different orientation of the molecular rows (dotted black lines) is clearly observed. Figure 4f depicts a profile of the lateral force traced along the horizontal marked line in Figure 4e. The characteristic saw-tooth shape profile of the stick-slip behavior reflects the periodic order of the molecular rows (scheme in Figure 4b).

A similar protocol as the above presented for pentacene was followed on this PTCDI-C8 surface. In this case, the whole experiments were performed in the attractive regime because slight load increase was observed to lead to an irreversibly damage of the molecular packing. In spite of these differences, the protocol also resulted in the nucleation and growth of new PTCDI-C8 layers on top of the initial surface film. This is exemplified in Figure 5 with representative frames illustrating the growth of islands up to the 6$^{th}$ layer.

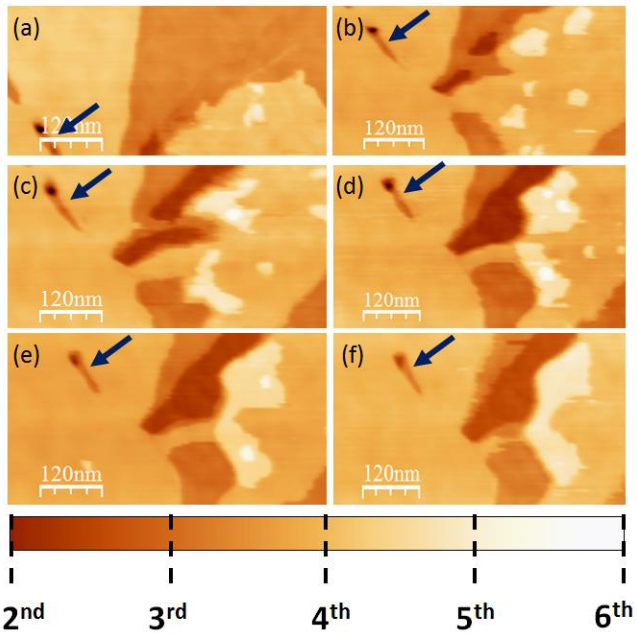

**Figure 5**: Selected topographic images of a PTCDI-C8 tip-induced growth. (a-f) correspond to frames number 1, 4, 5, 8, 11 and 12 of a total of 12.The fragmented color scale indicates the height of each molecular layer (2.2 nm). Dark arrows indicate the same defect in all the images.

As a reference for the morphological evolution, the same surface defect has been marked by arrows in all the images. Note that no bare $SiO_2$ exists and the lower level in the images corresponds to the second molecular layer. A difference from pentacene, where the material was transferred from the loading region to a distant and non-modified location, for PTCDI-C8 the growth process takes place by re-deposition of molecules close to the location from where they were removed. Thus, for instance, in Figure 5b molecules removed from the third layer and, therefore, leaving uncovered small areas of the second one (darker), are dragged by the tip and deposited at the top of the fourth layer. The subsequent growth of islands ($5^{th}$ and $6^{th}$ levels) proceeded during the course of the experiment. As above mentioned, conversely to pentacene, PTCDI-C8 films were considerably more vulnerable under the sweeping effect of the tip and some of the formed islands with smallest size eventually vanished. This is the case of some tiny islands of the $6^{th}$ level which are seen in Figure 5d but no longer appears in Figure 5f.

In fact, our observations imply molecular loading from the edges of inferior levels and incorporation at the terrace of nearby surfaces of the higher levels with no evidences of the opposite effect. The vicinity range of the process is illustrated in Figure 6 where two topographic AFM images before (a) and after (b) tip-induced modification are displayed.

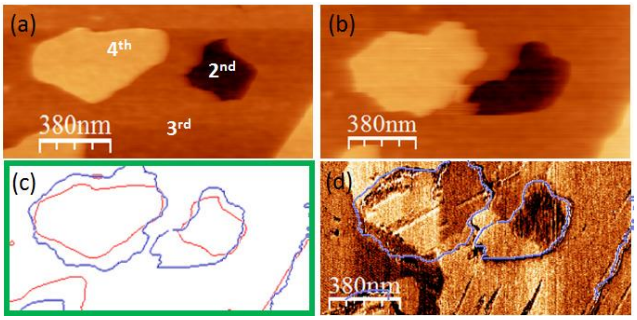


**Figure 6**: Topographic images of the same area before (a) and after (b) modification of the PTCDI-C8 film. (c) Relief contour plot corresponding to (a) in red and (b) in blue. (d) The TSM image corresponding to the topography in (b).

In this particular case, the formation of the 4$^{th}$ molecular layer occurs at expenses of the 3$^{rd}$ layer. This is reflected by an increase of the area of the pre-existing hole and an enlargement of the island size. To highlight these changes in topography, the relief contour outline for both images are merged in Figure 6c (red and blue for 6a and 6b, respectively). The friction anisotropy of PTCDI-C8 reflected in the TSM images allows inferring information on the crystallinity of the molecular layers and, particularly, whether the incorporated molecules adopt or not the azimuthal packing of the pre-existing island. The TSM image corresponding to the final stage of growth is shown in Figure 6d. As commented before, the TSM image reveals the domain boundaries between molecular domains with different azimuthal orientation. Comparison with the corresponding topographic contour superimposed to the TSM signal helps further interpretation. Note that a new region of the second layer has been uncovered after the modification revealing a grain boundary. The TSM signal of PTCDI-C8 assembled at the border of the 4$^{th}$ level island, replicates the signal of the underlying layer. Therefore, we can conclude that the molecules dragged and delivered by the tip on the surface reassemble in registry with the

same molecular orientation of the layer underneath rather than following the molecular orientation of the island at which they laterally attach.

**Conclusions**

We present a controlled tip-assisted manipulation allowing high quality 3D nanostructuration of ultrathin organic films. Using first the archetypal organic semiconductor pentacene and extending the investigation to PTCDI-C8, we have proved that the proposed procedure leads to high crystalline and homogeneous layers. A two-steps process, in which molecules at the initial film are loaded and posteriorly delivered back to the surface, is at the origin of our observations. The quality and stacking sequence of the growing layers are demonstrated by combining topographic and frictional data obtained in two different measuring geometries, namely FFM and TSM. The tip-induced grown molecular layers are crystalline. Whereas diverse stacking sequences have been observed in pentacene by means of FFM, the high contrast lateral force signal in TSM for PTCDI-C8 has permitted demonstrating that the molecular domains in the newly created layers are oriented in registry with respect to the underlying one. This result implies that the formed PTCDI-C8 assemblies replicate the in-plane orientation of the underlying film regardless of the orientation of the molecules in pre-existing islands to whose edges they are incorporated. As a consequence, though intra-layer domain boundaries may be created, a good 3D crystalline order is achieved. The capability of inducing the crystalline growth of molecular layers by AFM nanolithography could help on the nanostructuration of future organic nanodevices, i.e. OFETs with nanoscale channel lengths.

ASSOCIATED CONTENT

**Supporting Information** : Additional atomic force microscopy data including topographic and friction images are provided. The following file is available free of charge.

AUTHOR INFORMATION

Corresponding Author

* E-mail: ebarrena@icmab.es.

Present Addresses:

‡ Catalan Institute of Nanoscience and Nanotechnology (ICN2), CSIC and BIST, Campus UAB, Bellaterra, 08193 Barcelona, Spain

Author Contributions

The manuscript was written through contributions of all authors that have given approval to the final version of the manuscript. A. Pérez-Rodriguez and M. Paradinas contributed in the same manner to this work.

ACKNOWLEDGMENT

We thank M. Aghamohammadi for her help with the films growth. This work has been supported by the Spanish Government under projects MAT2013-47869-C4-1-P and MAT2016-77852-C2-1-R (AEI/FEDER, UE) and the Generalitat de Catalunya 2014 SGR501. We acknowledge the MINEICO project MAT2015-68994-REDC and the ‘‘Severo Ochoa’’ Program for Centers of Excellence in R&D (SEV-2015-0496). M. Paradinas thanks the Spanish

Government for financial support through BES-2008-003588 FPI and PTA2014-09788-I fellowships

REFERENCES

(1) Loos, J.; Alexeev, A. Scanning Probe Microscopy on Polymer Solar Cells. In *Applied Scanning Probe Methods X: Biomimetics and Industrial Applications*; Bhushan, B., Tomitori, M., Fuchs, H., Eds.; Springer Berlin Heidelberg: Berlin, Heidelberg, 2008; pp 183–215.

(2) Tseng, A. A.; Notargiacomo, A.; Chen, T. P. Nanofabrication by Scanning Probe Microscope Lithography: A Review. *J. Vac. Sci. Technol. B Microelectron. Nanom. Struct.* **2005**, *23*, 877–894.

(3) Rosa, L. G.; Liang, J. Atomic Force Microscope Nanolithography: Dip-Pen, Nanoshaving, Nanografting, Tapping Mode, Electrochemical and Thermal Nanolithography. *J. physics. Condens. matter.* **2009**, *21*, 483001–483018.

(4) Rubio-sierra, B. F. J.; Heckl, W. M.; Stark, R. W. Nanomanipulation by Atomic Force Microscopy. *Adv. Eng. Mater.* **2005**, *7*, 193–196.

(5) Piner, R. D. "Dip-Pen" Nanolithography. *Science.* **1999**, *283* (5402), 661–663.

(6) Shekhah, O.; Roques, N.; Mugnaini, V.; Munuera, C.; Ocal, C.; Veciana, J.; Wöll, C. Grafting of Monocarboxylic Substituted Polychlorotriphenylmethyl Radicals onto a COOH-Functionalized Self-Assembled Monolayer through Copper (II) Metal Ions. *Langmuir* **2008**, *24*, 6640–6648.

(7) Shekhah, O.; Wang, H.; Paradinas, M.; Ocal, C.; Schuepbach, B.; Terfort, A.; Zacher, D.; Fischer, R. A.; Woell, C. Controlling Interpenetration in Metal-Organic Frameworks by Liquid-Phase Epitaxy. *Nat. Mater.* **2009**, *8*, 481–484.

(8) Xu, S.; Liu, G. Y. Nanometer-Scale Fabrication by Simultaneous Nanoshaving and Molecular Self-Assembly. *Langmuir* **1997**, *13*, 127–129.

(9) Barrena, E.; Ocal, C.; Salmeron, M. Structure and Stability of Tilted-Chain Phases of Alkanethiols on Au(111). *J. Chem. Phys.* **2001**, *114*, 4210–4214.

(10) Barrena, E.; Palacios-Lidó, E.; Munuera, C.; Torrelles, X.; Ferrer, S.; Jonas, U.; Salmeron, M.; Ocal, C. The Role of Intermolecular and Molecule-Substrate Interactions in the Stability of Alkanethiol Nonsaturated Phases on Au(111). *J. Am. Chem. Soc.* **2004**, *126*, 385.

(11) Munuera, C.; Puigmartí-Luis, J.; Paradinas, M.; Garzón, L.; Amabilino, D. B.; Ocal, C. Layer-by-Layer Electropeeling of Organic Conducting Material Imaged in Real Time. *Small* **2009**, *5*, 214–220.

(12) Lyuksyutov, S. F.; Vaia, R. A.; Paramonov, P. B.; Juhl, S.; Waterhouse, L.; Ralich, R. M.; Sigalov, G.; Sancaktar, E. Electrostatic Nanolithography in Polymers Using Atomic Force Microscopy. *Nat. Mater.* **2003**, *2*, 468–472.

(13) Day, H. C.; Allee, D. R. Selective Area Oxidation of Silicon with a Scanning Force Microscope. *Appl. Phys. Lett.* **1993**, *62* (21), 2691–2693.

(14) Moreno, C.; Munuera, C.; Valencia, S.; Kronast, F.; Obradors, X.; Ocal, C. Reversible Resistive Switching and Multilevel Recording in La 0.7Sr0.3MnO3 Thin Films for Low

Cost Nonvolatile Memories. *Nano Lett.* **2010**, *10*, 3828–3835.

(15) Panzer, M. J.; Newman, C. R.; Frisbie, C. D. Low-Voltage Operation of a Pentacene Field-Effect Transistor with a Polymer Electrolyte Gate Dielectric. *Appl. Phys. Lett.* **2005**, *86*, 1–3.

(16) Rivnay, J.; Jimison, L. H.; Northrup, J. E.; Toney, M. F.; Noriega, R.; Lu, S.; Marks, T. J.; Facchetti, A.; Salleo, A. Large Modulation of Carrier Transport by Grain-Boundary Molecular Packing and Microstructure in Organic Thin Films. *Nat. Mater.* **2009**, *8*, 952–958.

(17) Gsänger, M.; Oh, J. H.; Könemann, M.; Höffken, H. W.; Krause, A. M.; Bao, Z.; Würthner, F. A Crystal-Engineered Hydrogen-Bonded Octachloroperylene Diimide with a Twisted Core: An N-Channel Organic Semiconductor. *Angew. Chemie - Int. Ed.* **2010**, *49*, 740–743.

(18) Minder, N. A.; Lu, S.; Fratini, S.; Ciuchi, S.; Facchetti, A.; Morpurgo, A. F. Tailoring the Molecular Structure to Suppress Extrinsic Disorder in Organic Transistors. *Adv. Mater.* **2014**, *26*, 1254–1260.

(19) Schmidt, R.; Oh, J. H.; Sun, Y.; Deppisch, M.; Krause, A.; Braunschweig, H.; Ko, M.; Erk, P.; Bao, Z.; Wu, F. High-Performance Air-Stable N-Channel Organic Thin Film Transistors Based on Halogenated Perylene Bisimide Semiconductors High-Performance Air-Stable N-Channel Organic Thin Film Transistors Based on Halogenated Perylene. *J. Am. Chem. Soc.* **2009**, *131*, 6215–6228.

(20) Struijk, C. W.; Sieval, A. B.; Dakhorst, J. E. J.; Dijk, M. Van; Koehorst, R. B. M.;

Donker, H.; Schaafsma, T. J.; Picken, S. J.; Craats, A. M. Van De; Warman, J. M.; et al. Liquid Crystalline Perylene Diimides : Architecture and Charge Carrier Mobilities. *J. Am. Chem. Soc.* **2000**, *122*, 11057–11066.

(21) Perez-Rodriguez, A.; Barrena, E.; Fernández, A.; Gnecco, E.; Ocal, C. A Molecular–scale Portrait of Domain Imaging in Organic Surfaces. *Nanoscale* **2017**, *9*, 5589–5596.

(22) Horcas, I.; Fernández, R.; Gómez-Rodríguez, J. M.; Colchero, J.; Gómez-Herrero, J.; Baro, A. M. WSXM: A Software for Scanning Probe Microscopy and a Tool for Nanotechnology. *Rev. Sci. Instrum.* **2007**, *78*, 13705.

(23) Kalihari, V.; Tadmor, E. B.; Haugstad, G.; Frisbie, C. D. Grain Orientation Mapping of Polycrystalline Organic Semiconductor Films by Transverse Shear Microscopy. *Adv. Mater.* **2008**, *20*, 4033–4039.

(24) Puntambekar, K.; Dong, J.; Haugstad, G.; Frisbie, C. D. Structural and Electrostatic Complexity at a Pentacenc/insulator Interface. *Adv. Funct. Mater.* **2006**, *16*, 879–884.

(25) Kalihari, V.; Ellison, D. J.; Haugstad, G.; Frisbie, C. D. Observation of Unusual Homoepitaxy in Ultrathin Pentacene Films and Correlation with Surface Electrostatic Potential. *Adv. Mater.* **2009**, *21*, 3092–3098.

(26) Fritz, S. E.; Martin, S. M.; Frisbie, C. D.; Ward, M. D.; Toney, M. F. Structural Characterization of a Pentacene Monolayer or an Amorphous SiO2 Substrate with Grazing Incidence X-Ray Diffraction. *J. Am. Chem. Soc.* **2004**, *126*, 4084–4085.

(27) Ruiz, R.; Choudhary, D.; Nickel, B.; Toccoli, T.; Chang, K. C.; Mayer, A. C.; Clancy, P.; Blakely, J. M.; Headrick, R. L.; Iannotta, S.; et al. Pentacene Thin Film Growth. *Chem.*

*Mater.* **2004**, *16*, 4497–4508.

(28) Mannsfeld, S. C. B.; Virkar, A.; Reese, C.; Toney, M. F.; Bao, Z. Precise Structure of Pentacene Monolayers on Amorphous Silicon Oxide and Relation to Charge Transport. *Adv. Mater.* **2009**, *21*, 2294–2298.

(29) Nickel, B.; Barabash, R.; Ruiz, R.; Koch, N.; Kahn, A.; Feldman, L. C.; Haglund, R. F.; Scoles, G. Dislocation Arrangements in Pentacene Thin Films. *Phys. Rev. B - Condens. Matter Mater. Phys.* **2004**, *70*, 125401–125407.

(30) Zhang, J.; Wu, Y.; Duhm, S.; Rabe, J. P.; Rudolf, P.; Koch, N. Formation of Intra-Island Grain Boundaries in Pentacene Monolayers. *Phys. Chem. Chem. Phys.* **2011**, *13*, 21102–21108.

(31) Hisada, K.; Knobler, C. M. Friction Anisotropy and Asymmetry Related to the Molecular Tilt Azimuth in a Monolayer of Glycerol Ester. *Langmuir* **2000**, *16*, 9390–9395.

(32) Liley, M. Friction Anisotropy and Asymmetry of a Compliant Monolayer Induced by a Small Molecular Tilt. *Science.* **1998**, *280*, 273–275.

(33) Carpick, R. W.; Sasaki, D. Y.; Burns, A. R. Large Friction Anisotropy of a Polydiacetylene Monolayer. *Tribol. Lett.* **1999**, *7*, 79–85.

(34) Gnecco, E.; Bennewitz, R.; Gyalog, T.; Meyer, E. Friction Experiments on the Nanometre Scale. *J. Physics-Condensed Matter* **2001**, *13* (31), 619–642.

(35) Paradinas, M.; Munuera, C.; Silien, C.; Buck, M.; Ocal, C. Heterogeneous Nanotribological Response of Polymorphic Self-Assembled Monolayers Arising from Domain and Phase Dependent Friction. *Phys. Chem. Chem. Phys.* **2013**, *15*, 1302–1309.

(36) Gourdon, D.; Burnham, N. A.; Kulik, A.; Dupas, E.; Stamou, D.; Liley, M.; Vogel, H.; Duschl, C.; Oulevey, F.; Gremaud, G.; et al. The Dependence of Friction Anisotropies on Themolecular Organisation of LB Films as Observed by AFM. *Trib. Lett.* **1997**, *3*, 317–324.

(37) Xie, X. N.; Chung, H. J.; Sow, C. H.; Wee, A. T. S. Nanoscale Materials Patterning and Engineering by Atomic Force Microscopy Nanolithography. *Mater. Sci. Eng. R Reports* **2006**, *54*, 1–48.

(38) Nita, P.; Pimentel, C.; Luo, F.; Milián-Medina, B.; Gierschner, J.; Pina, C. M.; Gnecco, E. Molecular Resolution Friction Microscopy of Cu Phthalocyanine Thin Films on Dolomite (104) in Water. *Nanoscale* **2014**, *6*, 8334–8339.

(39) Krauss, T. N.; Barrena, E.; Zhang, X. N.; de Oteyza, D. G.; Major, J.; Dehm, V.; Würthner, F.; Cavalcanti, L. P.; Dosch, H. Three-Dimensional Molecular Packing of Thin Organic Films of PTCDI-C8 Determined by Surface X-Ray Diffraction. *Langmuir* **2008**, *24*, 12742–12744.

(40) Krauss, T. N.; Barrena, E.; De OteyzaDimas, G.; Zhang, X. N.; Major, J.; Dehm, V.; Würthner, F.; Dosch, H. X-Ray/atomic Force Microscopy Study of the Temperature-Dependent Multilayer Structure of PTCDI-C8 Films on SiO2. *J. Phys. Chem. C* **2009**, *113*, 4502–4506.

(41) Aghamohammadi, M.; Fernández, A.; Schmidt, M.; Pérez-Rodríguez, A.; Goñi, A. R.; Fraxedas, J.; Sauthier, G.; Paradinas, M.; Ocal, C.; Barrena, E. Influence of the Relative Molecular Orientation on Interfacial Charge-Transfer Excitons at Donor/acceptor Nanoscale Heterojunctions. *J. Phys. Chem. C* **2014**, *118*, 14833–14839.

**TOC graphic**